Chapter 1
Applications of Remote Sensing for Air Pollution Monitoring in Thailand: An Early Warning for Public Health

Arika Bridhikitti

Abstract There are also consistent findings on the adverse effects of air pollution on public health in Thailand. Small size particulate matter, or $PM_{2.5}$, is the most pronounced air pollutant during the haze crisis. $PM_{2.5}$ often comes along with other polluted gases, including carbon monoxide (CO), oxides of nitrogen ($NO_x = NO + NO_2$), sulfur dioxide (SO_2), ozone (O_3), and volatile organic compounds (VOCs). This chapter presents various applications of remote sensing technology for air pollution monitoring, warning, and forecasting. These applications can help assess human exposure to air pollution and determine health risks associated with air pollution. The presentation is divided into four sections. The first section provides an overview of Earth Observing Satellites and current remote sensing technology for air pollution observations. The second section is on assessing the magnitude of atmospheric pollutants and human exposure levels from remote sensing. The third section is on air pollution source identification using remote sensing technology. Finally, the fourth section discusses the possibility of employing satellite information for forecasting haze episodes as the early warning tool. The presentation is based on the recent deployment of remote sensing technology for air pollution monitoring, especially reported for the cases of Thailand and the Southeast Asian region.

Keywords Satellite · Remote sensing · Air quality forecast · Air pollution · Particulate matter · Southeast Asia

A. Bridhikitti (✉)
Earth Science Research Cluster, Mahidol University Kanchanaburi Campus, 199 Moo 9, Lumsum Sub-District, Saiyok District, Kanchanaburi 71150, Thailand
e-mail: arika.bri@mahidol.edu

Environmental Engineering and Disaster Management Program, School of Interdisciplinary Studies, Mahidol University Kanchanaburi Campus, 199 Moo 9, Lumsum Sub-District, Saiyok District, Kanchanaburi 71150, Thailand

1.1 Introduction

Air pollution in Thailand has become public attention nowadays. In the dry season from December to March, the pollution is often reported at harmful levels, exceeding the national air quality standard. Pinichka et al. [1] studied the burden of disease attributed to air pollution and found that NO_2 and $PM_{2.5}$ could account for 10% and 7.5%, respectively, of the disease burden for all mortality. The $PM_{2.5}$ could also contribute to 16.8% of lung cancer cases and 14.6% of cardiovascular cases, whereas the NO_2 was responsible for 7.8% of respiratory mortality [1]. Jenwith-eesuk et al. [2] also showed evidence on $PM_{2.5}$-induced risk of colon cancer, with 15% risk increased for every ten micrograms $PM_{2.5}$ m^{-3} increased. Furthermore, US researchers have strong evidence showing that short-term exposure to $PM_{2.5}$ could significantly increase the risk of COVID-19 cases and death [3]. Not only the small-size aerosol, but the coarse-size particulate matter (PM_{10}) could also suddenly increase in hospital admissions as found a strong association between the PM_{10} level and the number of cardiovascular and respiratory admission in Bangkok, the most populated city in Thailand [4].

The Thai Government set up several policies and solutions to tackle haze pollution. The haze mitigation policy includes inspection and maintenance of vehicles, mandating higher quality fuel, and balancing productivity and environmental conservation in agricultural production [5]. During the haze episode, the policy relied on single command-and-control, framed by the central and provincial government [6]. The policies include prohibiting biomass burning, applying water sprays in public areas, roadside inspection on vehicle exhaust emissions, etc. [7]. Moran et al. [5] criticized that key issues of unsuccessful haze abatement in Thailand are low public participation and poor enforcement of laws or regulations. Scientists recommended policy outlines to minimize health effects from air pollution in the short term and eliminate the haze in the long run. The policy outlines included improvement of capacities to monitor, assess source inventory, and forecast air pollution, probably by incorporating applications of satellite retrievals in combination with ground measurements to fill spatial monitoring gaps [7, 8].

Satellite technology is widely applied for environmental monitoring since it provides spatial advantages for understanding the atmosphere and the land surface at the corresponding timeframe. Since air pollution is mainly released from surface activities, satellite observations could be helpful to provide strong connections between hot spots and pollution plumes or between urban land cover and heat island zone. The satellites could have multiple sensors onboarded, and each sensor was designed to capture specific radiative bands with certain viewing angles. Many Earth Observing Satellites detect solar reflectance and long-wave radiation from the Earth. These electromagnetic spectrums are appropriate for observing Ozone, Aerosol, Hydrocarbons, Greenhouse Gases, and Water vapor in the atmosphere. Some satellite sensors, such as Multiangle Imaging Spectroradiometer (MISR) and Cloud-Aerosol Lidar with Orthogonal Polarization (CALIOP), provide aerosol optical properties, beneficial for aerosol source identification. Furthermore, ground-based remote

sensing, such as Aerosol Robotic Network or AERONET, is typically used to validate satellite products. It can provide scattering and extinction properties of the atmospheric aerosols with a high temporal resolution by tracking direct sun and sky radiances.

1.2 Overview Earth Observing Satellites and Current Remote Sensing Technology for Air Pollution Observations

1.2.1 Earth Observing Satellites

By observing the Earth at the top of the atmosphere, satellite remote sensing can provide aerosol and gaseous compositions in the total atmospheric column basis. With approximately 1 μm and smaller, the aerosol highly scatters the energy spectrum in the visible to the near-infrared band from 300 to 1,000 nm. In addition, some types of aerosol absorb energy. The absorbing aerosols include black carbon (absorb both solar and thermal radiation) and mineral dust (scatter sunlight but absorb thermal infrared) [9]. The spectrophotometer is designed to observe solar radiation, and it can measure the extinction (both scattering and absorption) of the solar beam attributed to aerosol, called aerosol optical depth (AOD). Several satellite sensors have been previously employed for the studies of air pollution monitoring and assessment in Thailand. The summary of those sensors is detailed in Table 1.1.

Among the satellites, A-train (afternoon train) satellite constellation can be advantageous for atmospheric observation due to its combining multiple satellite remote sensors to better understand atmospheric and land dynamics. The constellation recently consisted of four satellites, orbiting in sequences, which are OCO-2 (launched in 2014), GCOM-W1 (since 2012), AQUA (since 2002), and AURA (since 2004) [10]. The satellites cross the equator around 1:30 PM local time with a 16-day repeating cycle.

The OCO-2 stands for Orbiting Carbon Observatory-2. The primary mission of OCO-2 is to quantify atmospheric carbon dioxide by its absorption of the visible band [11]. The GCOM-W1 stands for the Global Change Observation Mission-Water Satellite 1. It can explain the water cycle and climate change by observing the atmosphere and water bodies [12]. The GCOM-W1 is onboard with the Advanced Microwave Scanning Radiometer 2 (AMSR2), detecting microwave radiated from the ground, the water surface, and atmospheric gases, primarily greenhouse gases and water [12]. AQUA is designed to provide information about the Earth's hydrosphere. Furthermore, AQUA also enables the observation of aerosol via Moderate Resolution Imaging Spectroradiometer (MODIS) instrument and greenhouse gases via the Atmospheric Infrared Sounder (AIRS) along with the Advanced Microwave Sounding Unit (AMSU-A). AURA consists of four instruments to provide comprehensive studies on stratospheric and tropospheric compositions, including ozone,

Table 1.1 Summary of satellite sensors typically used for air pollution monitoring in Thailand

Sensors	Satellite	Standard detecting air pollution products	Temporal resolution	Spatial resolution, m	Reference
Moderate Resolution Imaging Spectrophotometer (MODIS)	TERRA since 2000, AQUA since 2002	Aerosol optical depth with a combined land and ocean algorithms	Level 2: Daily Level 3: Daily, 8-day, Monthly	Level 2: 10 km × 10 km (at nadir) Level 3: 1° × 1°	NASA Atmosphere Discipline Team Imager Products, https://modis-images.gsfc.nasa.gov/products.html
		Aerosol optical depth with dark target and deep blue algorithm	Level 2: Daily Level 3: Daily, 8-day, Monthly	Level 2: 10 km × 10 km (at nadir) and 3 km × 3 km (at nadir) Level 3: 1° × 1°	
		Aerosol optical depth with Multi-Angle Implementation of Atmospheric Correction, or MAIAC, algorithm	Daily	Level 2: 1 km × 1 km (at nadir)	
Measurements of Pollution in the Troposphere (MOPITT)	TERRA since 2000	CO Total Column	Daily, Monthly	Level 3: 1° × 1° horizontally, 10-level vertical (surface, 900 hPa, 800 hPa, ..., 100 hPa)	NASA TERRA, https://terra.nasa.gov/about/terra-instruments/mopitt
		CO Mixing Ratio for the layer above each pressure level			
		CO Mixing Ratio at the surface			

Table 1.1 (continued)

Sensors	Satellite	Standard detecting air pollution products	Temporal resolution	Spatial resolution, m	Reference
Multi-angle Imaging Spectroradiometer (MISR)	TERRA since 2000	Aerosol Optical Depth at 550 nm (also *including absorption, non-spherical, small-mode, medium-mode, large-mode*) Ångström Exponent at 550 and 860 nm	Level 3: Daily, Monthly, Quarterly, and Yearly	Level 2: 4.4 km × 4.4 km Level 3: 0.5° × 0.5°	NASA Jet Propulsion Laboratory, California Institute of Technology, https://misr.jpl.nasa.gov/
Ozone Monitoring Instrument (OMI)	AURA since 2004	Total column ozone: DOAS technique	Level 3: daily, monthly	Level 2: 13 km × 48 km at nadir Level 3d: 1° × 1° Level 3e: 0.25° × 0.25°	[16]
		Total column ozone: TOMS version 8 method			
		Aerosol: near UV algorithm			
		Aerosol: multi-wavelength algorithm			
		Ozone profile			
		Total column SO$_2$, HCHO, BrO, OClO, NO$_2$			

Table 1.1 (continued)

Sensors	Satellite	Standard detecting air pollution products	Temporal resolution	Spatial resolution, m	Reference
Cloud-Aerosol Lidar with Orthogonal Polarization (CALIOP)	CALIPSO since 2006	Aerosol Profile	Level 2: ~ 2 to 3 times per month	Level 2: 5 km × 5 km horizontal, 60 m vertical in the troposphere and 180 m vertical in the stratosphere	NASA, https://www-calipso.larc.nasa.gov/
		Vertical Feature Mask (including aerosol subtype)		Level 2: 5 km × 5 km horizontal, 1 km vertical (from 0 to 30 km)	
		Tropospheric Aerosol Profile (similar to Vertical Feature Mask)	Level 3: Monthly	Level 3: 2° latitude × 5° longitude, 60 m vertical from 0.5 to 12 km	

Table 1.1 (continued)

Sensors	Satellite	Standard detecting air pollution products	Temporal resolution	Spatial resolution, m	Reference
Visible Infrared Imaging Radiometer Suite (VIIRS)	Suomi NPP since 2011	Level 2 (or Environmental Data Record, EDR): aerosol optical thickness (AOT), aerosol particle size parameter (include Ångström exponent at 445 and 672 nm over land and at 865 and 1610 nm over the ocean), and suspended matter (include aerosol type and smoke concentration) Note: *available for Deep Blue and Dark Target algorithms as well*	Level 2: Daily Level 3: Daily, Monthly	Level 2: ~ 6 km × 6 km at nadir Level 3: $1^\circ \times 1^\circ$	[17–19]
		Aerosol data: Deep Blue Algorithm	Level 3: Daily, Monthly		

Note Level 1 is calibrated, and geolocated product, Level 2 is derived geophysical variables at the same resolution and location as Level 1 source data, or swath products, Level 3 is gridded variables in derived spatial and/or temporal resolutions

water, greenhouse gases, halogen compounds, oxides of nitrogen, carbon monoxide, and aerosols [13]. The AURA sensors include the High Resolution Dynamics Limb Sounder (HIRDLS), the Microwave Limb Sounder (MLS), the Ozone Monitoring Instrument (OMI), and the Tropospheric Emission Spectrometer (TES) [13].

Besides the AQUA satellite, the MODIS instrument is also onboard the TERRA satellite to provide a higher temporal resolution of the atmospheric aerosol. The TERRA passes to tropic at around 10.30 AM (ascending) and 10.30 PM (descending), whereas the AQUA is around 1.30 PM (ascending) and 1.30 AM (descending). Thus, their combined product can be provided four times daily. Even though aerosol observation can only perform in the daytime due to the requirement of light scattering, the nighttime satellite imagery can provide helpful information on socioeconomic parameters, such as population density and gross domestic product, and greenhouse gas emissions [14]. Thus MODIS product quite temporally advantages over other instruments and is universally employed for ground-level air pollution monitoring.

1.2.2   Ground-Based Remote Sensing

With currently more than 1,000 stations (see Fig. 1.1) and the number is growing, the AERONET (Aerosol Robotic Network, https://aeronet.gsfc.nasa.gov/) provided good spatial coverage of aerosol and cloud in the atmosphere. It is widely used as ground truth measurement for satellite retrievals of aerosol around the world. Currently, a total of 21 AERONET sites are based in Thailand. The AERONET program was established by the National Aeronautics and Space Administration (NASA), and LOA-PHOTONS, the French National Observatory for Aerosol, has been operated for more than 25 years. The AERONET aerosol products are measured by sun and sky photometers to measure direct and diffuse radiation. Details on the AERONET products are in Table 1.2. The aerosol products include spectral aerosol optical depth (AOD) and aerosol inversions, which provide aerosol microphysical and radiative properties. In parallel, the NASA Micro-Pulse Lidar Network (MPLNET: https://mplnet.gsfc.nasa.gov/) operates in conjunction with the AERONET to provide vertical integration structures of aerosol and cloud. The MPLNET project started with full operation in 2000. The MPLNET has three active sites in Thailand—Princess Sirindhorn Astro Park in the North, Silpakorn University in the Central, and Songkhla Regional Observatory in the South. Nonetheless, the current aerosol model cannot sufficiently describe vertical aerosol extinction measured during field campaigns over the Indian Ocean [15].
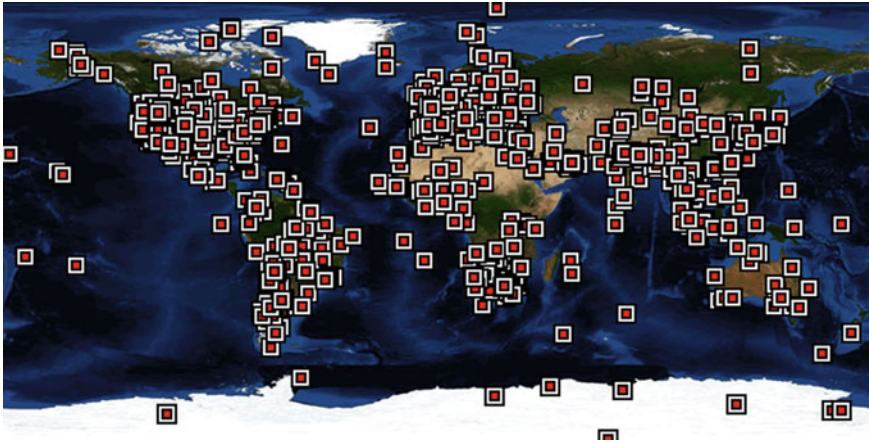
Fig. 1.1 AERONET sites (AERONET, 28 August 2021, retrieved from https://aeronet.gsfc.nasa.gov/)

Table 1.2 Products from direct sun measurements and aerosol optical properties from sun-sky photometers inversion products acquired from AERONET (https://aeronet.gsfc.nasa.gov/new_web/data.html)

AERONET products	Unit	Range
Direct sum measurement products		
Aerosol optical depth (AOD) Levels 1.0, 1.5, and 2.0, AOD (λ)	unitless	Level 1.0 unscreened Level 1.5 cloud screened Level 2.0 quality assured
Angstrom parameter, AE at 440–870 nm	Unitless	
Total water vapor at 940 nm	cm^3/cm^2 or $g\ cm^{-2}$	
Aerosol inversion products		
Volume particle size distribution, dV(r)/dlnr	$\mu m^3/\mu m^2$	$0.05\ \mu m \leq r \leq 15\ \mu m$
Volume concentration, C_v	$\mu m^3/\mu m^2$	For total, fine, and coarse aerosol modes Note: the fine and coarse separation point is the minimum within 0.439 to 0.992 μm
Volume median radius, r_v (mean logarithm of radius)	μm	
Standard deviation from r_v	μm	
Effective radius, r_{eff}	μm	
Real-part refractive index, n(λ)	Unitless	$\lambda = 440, 675, 870, 1{,}020$ nm 83 scattering angles, ~$7^o \leq \Theta \leq$ ~170°
Imaginary-part refractive index, k(λ)	Unitless	
Single scattering albedo, SSA(λ)	Unitless	
Phase function for each scattering angle, P(Θ, λ)	Unitless	
Asymmetry parameter for each phase function, cos(Θ)	Unitless	

1.3 Assessing Magnitude and Extents of Atmospheric Pollutants and Human Exposure Level from Remote Sensing

1.3.1 Tropospheric Ozone O_3 and Its Precursors

Once the tropospheric O_3 is generated, it can disintegrate into OH-radical. Though both the O_3 and OH-radical have short-lived in the environment, they have high oxidation potential, which can harm the soft tissues of plants, animals, and humans. Several previous studies confirmed that the O_3 could significantly increase human mortality [20–22]. The ozone is not directly emitted from the sources. It is the product of the photochemical reaction, in which the precursors mainly are NO_x and non-methane volatile organic compounds.

In Southeast Asia, biomass burning is the key source of O_3 and its precursors [23, 24]. Mekaumnuaychai et al. [25] and Yimlamaid et al. [26] employed satellite retrievals to assess the ozone precursors across Thailand. They found that the formaldehyde (HCHO) retrievals from the OMI/AURA satellite may not well reach the ground level, but the NO_2 retrievals from OMI/AURA and other satellites can represent the ground levels well in dry seasons [25, 26]. Furthermore, the UV radiation product of OMI can infer surface UV radiation with aerosol correction [27, 28]. The UV radiation provides energy driving photochemical reaction for O_3 generation in the troposphere. However, since the OMI provides total-column-based O_3, it may not sufficiently represent the ground levels. Tropospheric O_3 can be estimated by subtracting the OMI total column ozone with the MLS stratospheric ozone, which both OMI and MLS sensors are onboard the AURA satellite [24]. Thus, the data acquired from the OMI/MLS is recommended for assessing variation in tropospheric ozone and suggesting mechanisms for surface ozone control.

1.3.2 Aerosol Loading

Aerosol optical depth (AOD) is one of the aerosol optical products retrievable from satellites with visible to near-infrared band detectors. Satellite remote sensing is advantageous for studying long-term aerosol trends in regional to global scales [29]. Mehta et al. [29] employ satellite retrievals (both MODIS and MISR-Multiangle Imaging Spectroradiometer) for studying regional trends of aerosol magnitude. Their finding showed a noticeable increase in annual AOD over Southeast Asia from September to May, covering post- and pre-monsoon season [29]. The CSR, United States, attempts to predict air quality from MODIS AOD observation and to isolate local sources from the long-range transport sources using ground observation networks [30]. Though AOD is strongly affected by the amount of aerosol scattering and absorption, the AOD may not reach the ground level. The performance of the

new MODIS collection (6.1) aerosol products is spatially and temporally dependent [31]. The performance over the Asia continent is low, with less than 62% of the data sampling falling within the confidence intervals [31]. It could be likely due to the complex geography and various aerosol mixtures from natural and anthropogenic sources [31].

In northern Thailand, MODIS AOD was moderately-to-poorly correlated with ground-observed PM_{10}—$R^2 = 0.42$ during forest fire episodes [32] and $R^2 = 0.21$ for a normal episode [33]. Scientists and engineers have attempted to improve ground-level $PM_{2.5}$ prediction algorithm from satellite observation by developing empirical formula using multiple predictors, which is satellite-based AOD, land use, and meteorological variables, etc. With ground-based meteorological correction, the MODIS AOD at about 10:30 AM correlates better with the hourly ground-level $PM_{2.5}$ and PM_{10} using multiple linear regression ($R^2 = 0.74$), based on the study in Chiangmai, Thailand [33].

Since satellite retrievals are based on the pollutants' electromagnetic scattering and extinction properties in the atmospheric layer, they may not promise with the ground-based measurements using gravitational methods or chemical analytical methods. Nonetheless, satellite retrievals could be well responding to the ground during the high aerosol episode. Sayer et al. [34] studied corresponding between the MODIS collection 6 AOD and the AOD from ground-based sunphotometer measurements from Aerosol Robotic Network (AERONET) in the study at Doi Ang Khang, remote forest area in NW Thailand during the biomass burning episode. They found a strong correlation of R^2 0.93−0.94 [34]. The AERONET sun photometer employs the same approach like that of the satellites, considering aerosol optical properties. The correlations for board arrays of land covers and aerosol loadings were slightly declined as found to be R^2 of 0.81 for MODIS AOD and AERONET AOD and 0.68 for VIIRS/Suomi NPP AOD and AERONET AOD across the Southeast Asia region [35].

1.3.3 Biomass Burning Smoke

Biomass burning releases smoke plumes containing carbonaceous aerosol, CO_2, CO, NO_x, and other uncompleted burning products to the atmosphere [36]. The emission of biomass burning smoke in the Southeast Asian region is globally concerned in terms of its magnitude and its contribution to climate change [37]. The biomass burning contributes to 49% of total PM_{10} in Southeast Asian mainland, and the highest contribution was from Laos (73%), followed by Myanmar (69%), Cambodia (59%), Thailand (45%), China (33%) and Vietnam (31%) [37]. In Thailand, a total of 117.7 Mt of rice residue was left on the field after being harvested, and 15% of the amount was later burnt. The burning emitted approximately 2.19 Mt of combined air pollutants, and 30% of the amount was from the lower Northern Thailand, followed by central Thailand (26%) and western Thailand (17%) [36].

Satellite observations can provide reasonable estimates of smoke magnitude as found in the studies in northern Thailand. Sukitpaneenit and Oanh [32] monitored forest fire smoke using MODIS and Measurement of Pollution in the Troposphere (MOPITT) onboard TERRA satellite. They found that the MODIS AOD can capture variation in ground-measured PM_{10} by ~42% using a linear regression model, whereas the MOPITT CO can explain the ground-level CO by ~35%. Lalitaporn and Boonmee [38] employed tropospheric NO_2 column from SCIMACHY, OMI, GOME-2A, and GOME-2B sensors. They found that high levels of the NO_2 corresponded well with ground-level NO_2 ($R^2 = 0.29$ to 0.66) and a number of biomass burning hot spots.

1.4 Air Pollution Source Identification Using Remote Sensing Technology

1.4.1 Aerosol Optical Properties

Radiative sensors can sense atmospheric aerosols through their scattering and absorption of incoming solar radiation. With these optical properties, the aerosols can influence the Earth's radiative balance, either negative effect (cooling) or positive effect (warming), depending upon their composition, shape, size, and mixing state [9]. Absorbing aerosols include black carbon. The aerosol optical properties can be expressed from the single scattering albedo (SSA), aerosol optical depth (AOD), and Angström exponent (AE), etc. The SSA is the ratio of scattering coefficient to the extinction coefficient (combine scattering and adsorption effects). The AOD refers to the magnitude of aerosol by representing the depth of the direct solar beam lost when traveling through the aerosol layer [9]. AE is the log-slope exponent of the spectral aerosol optical depth between two wavelengths [39].

Recently, scientists have tried to simulate aerosol properties using various climate and aerosol models. Takemura et al. [39] employed an aerosol transport model coupled with an atmospheric general circulation model to simulate the SSA of primary aerosols—carbonaceous (organic and black carbons), sulfate, and soil dust and sea salt aerosols. Age aerosol with internal mixing (among the same type of aerosols) or external mixing (among different types) could exhibit lower SSA since its increasing adsorption efficiency. In contrast, the scattering efficiency is less affected by the mixing [39]. Different aerosol types can be distinguished by knowing the aerosol optical properties, as shown in Tables 1.3 and 1.4. Clean oceanic sea salt exhibits high light scattering (SSA of ~0.99, (Mallet et al. (2004) cited in [40]) and low light absorption (imaginary-part reflective index <0.001) [41]. Long-range transport urban/industrial aerosol from East Asia to Southeast Asia also exhibited high SSA of >0.95 (at 440 nm) and coarser fine mode size of >0.2 μm [42]. The high SSA could be due to the aerosol's hygroscopic growth and secondary aerosol formation along the air trajectory. Nonetheless, long-range transport of the polluted air masses

from NE Asia and SE Asia to the remote island, Mauna Loa in HAWAII, did not exhibit high scattering properties, suggesting its hydrophilic properties and insignificant secondary aerosol formation [43]. From January to April, the aerosol exhibited a lower SSA of approximately 0.90, a higher refractive index, and smaller fine-mode size, suggesting biomass burning smoke [42]. The urban aerosol exhibited a mean SSA of approximately 0.90 (440 nm) or lower. The coarse-mode aerosol, possibly road dust or soil dust, played a role from October to January when seasonal winds were strongest [42].

Scientists try to understand the aerosol optical properties and employ the knowledge to indicate the potential origins of the aerosols. There are many previous studies employing satellite retrievals to identify sources of aerosols, as the detail was given in the following sections.

1.4.2 Local Biomass Burning

Biomass burning is the key source of haze pollution in the Southeast Asia continent, including Thailand. Agricultural residue burning for land preparation occurs regularly before starting cropping season in May [5, 57]. In northern Thailand, forest fires can often be found with agricultural burning resulting in poor air quality in remote areas, such as Doi Ang Khang [34].

Remote sensing can be used to identify biomass burning sources of air pollution by its association among fire hotspots, air pollutant loading, and land cover. Kamthonkiat et al. [58] developed an empirical model using Landsat 8 imagery to estimate ground-measured PM_{10}. Their finding showed that the model is highly correlated with land use/cover, primarily agricultural land and forests, and fire hotspots. They conclude significant contributions of biomass burning in the air pollution in Nan, Thailand [58].

Consistently, the BASE-ASIA in 2006 and the 7-SEAS in 2010–13 campaigns were conducted over northern Southeast Asia by collaboration among the Southeast Asia START region center, NASA, and the University of Hawaii to understand aerosol and cloud properties in this region using satellite and *in-situ* measurements [59]. Based on the BASE-ASIA deployment over Thailand, Myanmar, and Laos, the result shows a good correlation ($R^2 = 0.66$) between the MODIS fire activity and MODIS AOD, suggesting a significant smoke from forest fires and agricultural crop burning [59]. Furthermore, Li et al. [52] presented comprehensive biomass-burning aerosol properties measured at a remote site of Phimai, in NE Thailand. The aerosol had dominant carbonaceous components and substantial loadings of SO_4^{2-}, NH_4^+, NO_3^-. The aerosol also had hygroscopic properties, enhancing aerosol light scattering and hygroscopic growth [59].

Table 1.3 Aerosol optical properties from the literature

Studied areas	Aerosol chemical compositions	Potential sources	Size	Angstrom exponent	SSA	AOD	Reference
The remote island, Mauna Loa in HAWAII	–	Long-range transport of dust and pollution aerosols from NE Asia in spring from March to May	Coarse	–	0.87 (550 nm)	–	[43]
		Biomass burning from SE Asia in spring from March to May	Fine	–	0.86 (550 nm)	–	
		Pacific Ocean	Fine	–	0.86 (550 nm)	–	
East Coast of US	Sulfate	Oceanic	0.18–0.21 µm 1.43–2.05 µm Geometric median diameter	–	0.96 ± 0.03 (550 nm)	0.13 ± 0.10	[44]
Thar Desert, Jodhpur India	High hematite content Moorthy et al. (2007) cited in Gogoi et al. (2013)	Desert dust With high absorption in Blue, UV, and IR	Coarse	0.71 ± 0.2	–	0.66 ± 0.14 (500 nm)	[45]

(continued)

Table 1.3 (continued)

Studied areas	Aerosol chemical compositions	Potential sources	Size	Angstrom exponent	SSA	AOD	Reference
Urban central China	–	Coal combustion (both local and transported) in winter Gas to particle conversion and hygroscopic growth of Nitrates, sulfates, and ammonium sulfates particles	Fine mode decreases from summer (0.23 μm) to spring (0.17 μm)	1.16–1.24 (440–870)	0.87 in winter 0.93 in summer Mean 0.89 (440 nm)	1.16–1.28	[46]
Kanpur, N India	–	Industries, coal thermal power plants, automobile exhausts, bio-fuel combustions, biomass burning in post-monsoon	0.2 μm, 2 μm	1.30 ± 0.11 (440–870 nm)	–	>0.93	[47]
		Local mineral dust in monsoon	2 μm	0.36 ± 0.41 (440 – 870 nm)	–	–	
Delhi, India in winter	–	Secondary (traffic) in the winter morning	$PM_{2.5}$	–	0.93 ± 0.03 (500 nm)	0.95 ± 0.32	[48]
Boreal forest, N Europe	–	Soil dust, sea salt	PM_{10}	1.80 ± 0.55 (450–700 nm)	0.87 ± 0.07 (550 nm)	–	[49]

(continued)

Table 1.3 (continued)

Studied areas	Aerosol chemical compositions	Potential sources	Size	Angstrom exponent	SSA	AOD	Reference
		Soil dust, sea salt, brown carbon (BC + OC) from wood burning in winter, and secondary reaction in summer	PM1	2.22 ± 0.44 (450–700 nm)	0.85 ± 0.08 (550 nm)	–	
Urban Beijing	–	Secondary reaction, cooking, traffic (day), diesel truck transport (night)	–	–	0.82, 0.77, 0.78 (670 nm)	–	[50]
Amazon Basin	–	Biomass burning	1.5 µm cut point	1.8 ± 0.2 (440–670 nm)	0.92 ± 0.02 (545 nm)	3.0	[51]
Laboratory	Sea salt	–	–	–	0.99	–	Mallet et al. (2004) cited in [40]
Coastal industrial areas, France	Sea salt + internally mixed with Black Carbon	–	–	–	0.75	–	
Coastal industrial areas, France	Sea salt + externally mixed with Black Carbon	–	–	–	0.85	–	
Remote Agricultural site, Phimai, NE Thailand	Black Carbon, Organic Carbon, K^+, SO_4^{2-}, NH_4^+, NO_3^-	Biomass burning	–	–	0.86 ± 0.04 to 0.92 ± 0.02 (550 nm)	–	[52]

(continued)

Table 1.3 (continued)

Studied areas	Aerosol chemical compositions	Potential sources	Size	Angstrom exponent	SSA	AOD	Reference
Indochina peninsula	–	Biomass burning	–	–	0.91 ± 0.02 (440–1020 nm) with the lowest over the northern location of Chiang Mai (−0.85)	–	[53]
Boreal forests or peatlands	–	Boreal forest fires Peat burning	Larger fine mode	–	0.95–0.97 (440–1020 nm)	–	[54]
Grasslands, Scrublands, Croplands	–	Biomass burning	Smaller fine mode	–	0.88–0.90 (440–1020 nm)	–	
Tropical forest, Alta Floresta, Brazil	–	Forest fires	Fine mode size, $\mu m = 0.151 + 0.0099\log(2.0 \times AOD_{fine}$ at 440 nm) Coarse mode size, $\mu m = 3.2\ \mu m$	1.95 for 440–870 nm	~ 0.92 (440–1020 nm)	3.78 (max at 440 nm)	
African Savannah, Mongu, Zambia	–	Savannah fires	Fine mode size, $\mu m = 0.175 + 0.012\log(0.12 \times AOD_{fine}$ at 440 nm) Coarse mode size, $\mu m = 3.34$	1.89 for 440–870 nm	~ 0.85 (440–1020 nm)	2.29 (max at 440 nm)	

(continued)

Table 1.3 (continued)

Studied areas	Aerosol chemical compositions	Potential sources	Size	Angstrom exponent	SSA	AOD	Reference
Bac Giang, Vietnam	–	Long-range transport urban/industrial aerosol	r_{eff}-F/C, μm = 0.226/2.465	1.268 for 440–870 nm	0.951/0.952/0.951/0.950 (440/675/870/1020 nm)	–	[42]
	–	Biomass burning smoke	r_{eff}-F/C, μm = 0.167/2.264	1.409 for 440–870 nm	0.900/0.899/0.899/0.897 (440/675/870/1020 nm)	–	
Mukdahan, NE Thailand	–	Biomass burning smoke	r_{eff}-F/C, μm = 0.172/2.453	1.544 for 440–870 nm	0.911/0.896/0.885/0.872 (440/675/870/1020 nm)	–	
	–	Long-range transport urban/industrial aerosol	r_{eff}-F/C, μm = 0.216/2.789	1.328 for 440–870 nm	0.950/0.943/0.937/0.931 (440/675/870/1020 nm)	–	
Pimai, NE Thailand	–	Biomass burning smoke	r_{eff}-F/C, μm = 0.168/2.472	1.541 for 440–870 nm	0.905/0.891/0.886/0.878 (440/675/870/1020 nm)	–	
	–	Long-range transport urban/industrial aerosol	r_{eff}-F/C, μm = 0.203/2.794	1.365 for 440–870 nm	0.950/0.946/0.945/0.942 (440/675/870/1020 nm)	–	
Silpakorn U., Central Thailand	–	Local urban/industrial aerosol	r_{eff}-F/C, μm = 0.156/2.386	1.560 for 440–870 nm	0.884/0.873/0.850/0.830 (440/675/870/1020 nm)	–	
	–	Biomass burning smoke	r_{eff}-F/C, μm = 0.170/2.257	1.536 for 440–870 nm	0.917/0.906/0.886/0.870 (440/675/870/1020 nm)	–	

(continued)

Table 1.3 (continued)

Studied areas	Aerosol chemical compositions	Potential sources	Size	Angstrom exponent	SSA	AOD	Reference
	–	Local urban/industrial aerosol with high fraction of soil dust	r_{eff}-F/C, µm = 0.192/2.990	1.274 for 870–440 nm	0.908/0.905/0.889/0.874 (440/675/870/1020 nm)	–	

Note Internal mixing = mixing among the same type of particles, External mixing = mixing with different types of particles

Table 1.4 Complex refractive indices of the aerosols reported in the literature

Aerosol type	Real (550 nm)	Imaginary (550 nm)	Reference
Water soluble	1.53	0.006	[41]
Dustlike	1.53	0.008	
Soot	1.75	0.44	
Oceanic	1.381	4.26×10^{-9}	
Clean continental (water soluble 48% + dustlike 52%)	1.53	0.00704	
Urban (water soluble 97.5% + dustlike 0.3% + soot 2.2%)	1.535	0.0156	
Maritime (water soluble 95% + Oceanic 5%)	1.388	0.0003	
Sea salt and aged sea salt (Cl + Na + S > 85%)	1.53	–	[55]
Ammonium sulfate (S > 85%)	1.53	–	
Silicates (Al + Si > 60%)	1.53	–	
Metal oxides/hydroxides (Al, Ti, Mn, Fe, Cu, Ni, Zn, Pb > 80%)	2.5	0.05	
Calcium sulfate (Ca > 30%, S > 40%)	1.53	–	
Carbonates (Ca > 60%, S < 20%)	1.53	–	
Soot	1.5	0.47	
Biological (minor elements: Na, Mg, P, S, Cl, K, Ca)	1.4	–	
Carbon/sulfate mixed particles (S > 15%)	1.5	0.05	
Rest of the carbon-rich particles	1.53	–	
Soil dust, sea salt in Boreal forest, N Europe	1.518 ± 0.067	0.02 ± 0.018	[49]
Soil dust, sea salt, brown carbon (BC + OC) from wood burning in winter and secondary reaction in summer in Boreal forest, N Europe	1.484 ± 0.054	0.025 ± 0.018	

Table 1.4 (continued)

Aerosol type	Real (550 nm)	Imaginary (550 nm)	Reference
Biomass burning aerosol (oxalic acid 0.6 μg m^{-3}, KNO$_3$ 0.8 μg m^{-3}, K$_2$SO$_4$ 1.3 μg m^{-3}, Ammonium sulphate 2.3 μg m^{-3}, Levoglucocsan 1.4 μg m^{-3}, EC 5.6 μg m^{-3}, OM 24.7 μg m^{-3})	1.54	0.013	[56]
Organic matters	1.4	–	
Elemental carbon	1.87	0.22	
Long-range transport urban/industrial aerosol (at 440/675/870/1020 nm)	1.403/1.416/1.423/1.418 at Bac Giang, Vietnam 1.402/1.416/1.423/1.420 at Mukdahan, NE Thailand 1.409/1.423/1.432/1.434 at Pimai, NE Thailand	0.007/0.006/ 0.005/0.005 at Bac Giang, Vietnam 0.007/0.007/ 0.007/0.007 at Mukdahan, NE Thailand 0.006/0.006/ 0.005/0.005 at Pimai, NE Thailand	[42]
Biomass burning smoke (at 440/675/870/1020 nm)	1.428/1.448/1.462/1.458 at Bac Giang, Vietnam 1.433/1.448/1.454/1.451 at Mukdahan, NE Thailand 1.423/1.437/1.450/1.445 at Pimai, NE Thailand 1.413/1.426/1.437/1.433 at Silpakorn U., C Thailand	0.014/0.011/ 0.010/0.009 at Bac Giang, Vietnam 0.014/0.013/ 0.012/0.013 at Mukdahan, NE Thailand 0.014/0.013/ 0.011/0.011 at Pimai, NE Thailand 0.012/0.011/ 0.011/0.012 at Silpakorn U., C Thailand	
Local urban/industrial aerosol (at 440/675/870/1020 nm)	1.469/1.480/ 1.487/1.480 at Silpakorn U., C Thailand	0.019/0.017/ 0.017/0.017 at Silpakorn U., C Thailand	

1.4.3 Urban Pollution

In urban areas, the source contributions cannot be easily identified due to multiple sources, complex ground reactions facilitated by urban heat island characteristics. The Economic and Social Commission for Asia and the Pacific (ESCAP), the United Nations conducted the studies to understand key sources of air pollution in the major cities in Thailand—Bangkok, Chiang Mai, and Nakhon Srithammarat. Their work incorporated both ground-based measurements (meteorological parameters and air quality index) and satellite retrievals (land cover and hotspots) into machine learning models [60]. The findings showed that biomass burning and forest fires are the primary sources in all cities, with minor contributions from urban activities [60].

1.4.4 Long-Range Transport Air Mass

Both ground-based sensing and satellite remote sensing are advantageous for estimating and tracking the extent of biomass burning smoke plumes. Duc et al. [57] employed the integrated data from AERONET, MODIS, and CALIPSO satellites to assess the extent of biomass burning smoke from the Southeast Asian mainland. They found that the smoke plumes could be transported to southern China, Taiwan, and farther. Smoke haze from the Southeast Asian Region can be evident and contribute to the air pollution problem on a global scale. NASA initiated the framework of biomass-burning Aerosols in Southeast Asia: Smoke Impact Assessment, or BASE-ASIA, in 2006 to evaluate the impact of the aerosols [61]. The BASE-ASIA employs various resources from numerical simulation, the analysis of AERONET aerosol optical properties from multiple sites, and satellite observation. From 2008 to 2013, Seven Southeast Asian Studies, or 7-SEAS, campaign were implemented [59]. Under the 7-SEAS campaign, the NASA scientists employed mobile laboratories and ground-based networks (both AERONET and MPLNET) [59]. From BASE-ASIA to 7-SEAS, scientists observed long-range transport of the smoke aerosols and understood dynamics of the aerosol optical properties along with trajectories, affecting climate warming or cooling.

Since polluted air masses can aloft and transport across the national boundaries. In such a case, the previous models developed using local parameters may not well explain these long-range transport air masses. Scientists and engineers use the advantages of CALIOP air products to observe vertical profiles of aerosol types and later employ backward trajectory models to track potential sources of aerosol clouds for individual cases. Bridhikitti [62] employed aerosol layer scenes taken from CALIOP over the Bangkok Metropolitan Region (BMR) and found that the long-range transport smoke was the most often found at the elevation of approximately 0.7–1.5 km (Fig. 1.2). The CALIOP aerosol profile also suggests long-range transport of polluted dust to the BMR at the elevated level of 3.0–3.2 km during monsoon season (June to September).

Backward trajectory analysis also assists in indicating sources of the long-range transport aerosol. For example, as seen from Fig. 1.3 in the work of [62], the smoke (in the left figure) aloft over the BMR could be transported from the E-to-SE Asian continent, and the polluted dust (in the right-hand figure) could be from S Asia. The HYSPLIT trajectory model from NOAA (https://www.ready.noaa.gov/HYSPLIT.php) is widely used interactively for computing the backward air parcel trajectories [62, 63].
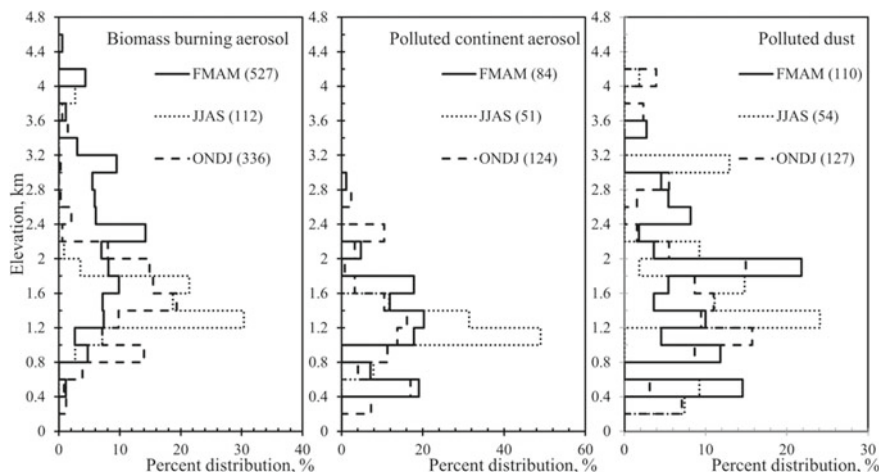
Fig. 1.2 Frequency distribution of aerosol top layer over Bangkok Metropolitan Region from CALIPSO Observations. *Note* FMAM = February to May, JJAS = June to September, ONDJ = October to January [62]

1.5 Satellite Retrievals for Forecasting Haze Episode as the Early Warning Tool

Current approaches for air quality forecasting are applications of chemical transport models, statistical methods, ground and satellite observation networks, and deep learning techniques [64]. The U.S. Environmental Protection Agency's AirNow program employs surface observations of PM2.5 for more than 500 cities to forecast Air Quality Index (AQI). The forecast also combines the satellite observations of aerosol from the Interagency Monitoring of Protected Visual Environments (IMPROVE) network to fill the gaps in the rural areas of the continental U.S. [65] Along with the forecasted AQI, the Chemical Speciation Network (CSN) has been operated to measure the chemical composition of ground-level PM in the urban areas for PM sources identifications [65]. Zhang et al. [65] also proposed the improvement of PM2.5 forecasts in the continental U.S. through the integrating uses of satellite retrievals (including AOD products from TERRA. AQUA, and VIIRS), multi-chemical transport models (including GEOS-Chem, WRF-Chem, and CMAQ), and ground observations. The integration was claimed to provide the best performance for today and next-day forecast [65]. Nonetheless, the study of air pollution episodes in Poland showed highly seasonal dependence and cloud effects on the forecasting performance [66]. From 2005 to 2009, European Commission funded the Global and Regional Earth-System Monitoring Using Satellite and In situ Data, or GEMS project. The project collaborates among researchers from eighteen research institutes in Europe to develop a pilot system for enhancing the forecasting capacity for
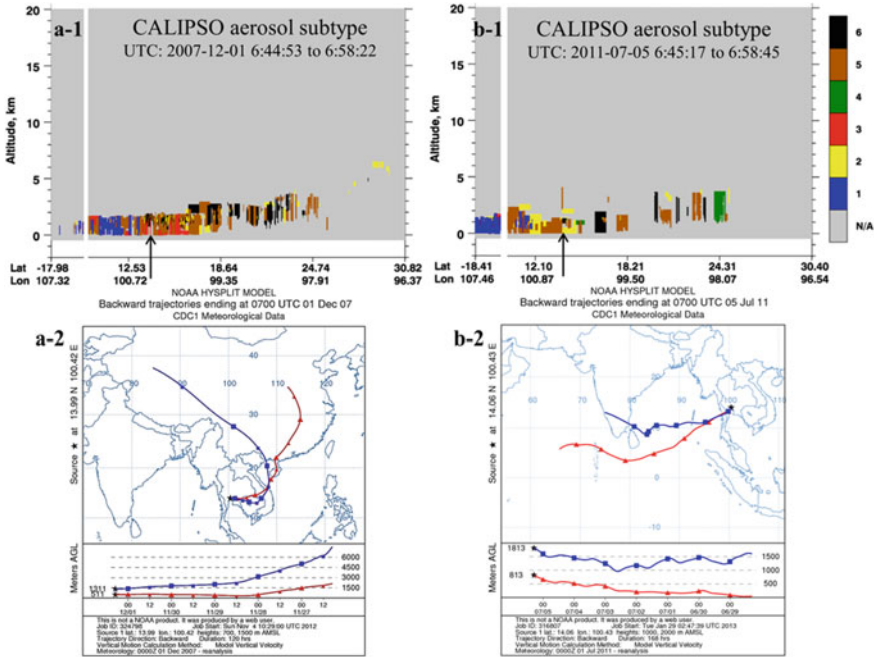
Fig. 1.3 CALIPSO aerosol subtypes (1 = clean marine, 2 = dust, 3 = polluted continental, 4 = clean continental, 5 = polluted dust, 6 = smoke, N/A = not applicable) for the daytime on December 1st, 2007 (**a-1**) and the daytime on July 5th, 2011 (**b-1**) and their corresponding HYSPLIT back trajectories at 13.99°N100.42°E (**a-2**, at 700 m above mean sea level for red line and 1,500 m for blue line) and at 14.06°N 100.43°E (**b-2**, at 1,000 m above mean sea level for red line and 2,000 m for blue line), respectively [62]

aerosols, greenhouse gases, and reactive gases in the atmosphere and improving forecasts for regional air quality [67]. The GEMS production required multi-satellite and remote sensing datasets for developing the best-fitted forecast model. The continuation of GEMS after 2009 was the Monitoring of Atmospheric Composition and Climate (MACC) project. One of the objectives of the MACC project was to provide information services on short-term forecast air quality for Europe [67].

Nowadays, the deep learning model gains more scientific attention for air quality forecast since it can extract complex interconnections using a large pool of ground-measured and satellite-based datasets. Sharma et al. [68] show that the deep learning model can be used to forecast satellite-based PM_{10}. The technique can be beneficial for early warning of hazards associated with air pollution from hotspots in Australia [68]. This method, however, is still in the early stage of development and its lack of interpretability needs to be accomplished to make the technique more useful [64].

In case of Thailand and the Southeast Asian Region, the application of satellite retrievals for air quality forecasting is recommended for remote areas with a sparse ground monitoring network [69]. Li et al. [69] developed a linear regression model

using MODIS AOD and ground-measured meteorological factors to predict PM_{10} levels in the next day. The model provided a percentage error of less than 30% for hindcasts for the cities in China and Thailand [69]. In 2020, SERVIR-Mekong, a partnership between the US Agency for International Development (USAID) and the US National Aeronautics and Space Administration (NASA), developed new web-based tool, which is "Mekong Air Quality Explorer Tool" to improve air quality monitoring and forecasting in Thailand and other countries in the Lower Mekong River Basin. Users can access and visualize 3-day $PM_{2.5}$ forecast derived from NASA GEOS global forecast model [70]. The forecast employs MODIS AOD from TERRA and AQUA satellites and fire products (fire radiative power and number of fires) from the MODIS and VIIRS/Suomi NPP. The forecast simulation for Thailand is bias corrected using machine learning algorithm [70]. The developer aims that the tools can facilitate decision-making on air quality management, especially in the haze season.

1.6 Summary

Satellite remote sensing has been widely used for air pollution monitoring nowadays primarily because it provides spatial advantages over ground-based monitoring. Previous studies in Thailand assessed the magnitude and extents of atmospheric pollutants from remote sensing. The studies had been focused on tropospheric O_3 and its precursors, aerosol loading, and pollutants from biomass burning. The observations, however, are primarily reported as the total atmospheric column, and in some cases, the retrievals may not reach the ground. Therefore, scientists are developing various algorithms using land surface properties and meteorological parameters to assess magnitudes of ground-level air pollutants from satellite retrievals. The temporal resolution of the satellite retrievals is another limitation. The limitation can be accomplished by employing the retrievals from multi-satellite having similar functioning sensors, such as MODIS/TERRA, MODIS/AQUA, and VIIRS/Suomi NPP. The integrated satellite retrievals also yield a better estimate of air pollutant magnitudes with different atmospheric heights. The retrievals from A-Train satellites can be superior since several satellites were orbiting in line, with the near corresponding timeframe. Furthermore, ground-based remote sensing network, such as AERONET for aerosol retrieval, is widely used to understand the dynamics of aerosol properties at particular locations and provide the data used for validating the satellite retrievals.

Using remote sensing technology to identify air pollution sources was successfully implemented in Thailand for biomass burning/wildfires, urban pollution, and long-range transport air masses. Algorithms for the source identification have been relied upon either multivariate analyses of the remote-sensing aerosol optical properties and/or justified from the co-presence of air pollutants as fingerprints for specific sources. The recent development of satellite data analysis for forecasting haze is ongoing. The development requires integrations among long-term satellite observations, surface measurements, and chemical transport models.

References

1. Pinichka C, Makka N, Sukkumnoed D, Chariyalertsak S, Inchai P, Bundhamcharoen K (2017) Burden of disease attributed to ambient air pollution in Thailand: a GIS-based approach. PLoS ONE 12(12):e0189909

2. Jenwitheesuk K, Peansukwech U, Jenwitheesuk K (2020) Accumulated ambient air pollution and colon cancer incidence in Thailand. Sci Rep 10(1):1–12

3. Zhou X, Josey K, Kamareddine L, Caine MC, Liu T, Mickley LJ, Cooper M, Dominici F (2021) Excess of COVID-19 cases and deaths due to fine particulate matter exposure during the 2020 wildfires in the United States. Sci Adv 7(33):eabi8789

4. Phosri A, Sihabut T, Jaikanlaya C (2020) Temporal variations of short-term effects of particulate matter on hospital admissions in the most densely populated city in Thailand. Sci Total Environ 742:140651

5. Moran J, NaSuwan C, Poocharoen OO (2019) The haze problem in northern Thailand and policies to combat it: a review. Environ Sci Policy 97:1–15

6. Tipayarat Y, Sajor EE (2012) State simplification, heterogeneous cause of vegetation fires and implication on local haze management: case study in Thailand. Environ Dev Sustain 14:1047–1064

7. Wongwatcharapaiboon J (2020) Toward future particulate matter situations in Thailand from supporting policy, network and economy. Future Cities Environ 6(1)

8. Shi H, Wang Y, Chen J, Huisingh D (2016) Preventing smog crises in China and globally. J Clean Prod 112:1261–1271

9. Liu Y, Jia R, Dai T, Xie Y, Shi G (2014) A review of aerosol optical properties and radiative effects. J Meteorol Res 28(6):1003–1028

10. Ferrier C, Boschetti M, Fourcade J, Gamet P, Gamet P (2010) Exit the A-Train constellation: PARASOL and CALIPSO different strategies. In: SpaceOps 2010 conference delivering on the dream hosted by NASA marshall space flight center and organized by AIAA, p 2275

11. Murphy R (2014) OCO-2 takes the A-Train to study earth's atmosphere. National Aeronautics and Space Administration. https://www.nasa.gov/jpl/oco2/a-train-atmosphere-20140703. Accessed on 17 October 2021

12. Kawaguchi M, Yoshida T (2013) Regular observation by global change observation mission 1st-water GCOM-W1 (Shizuku). NEC Tech J 8(1):32–35

13. Schoeberl MR, Douglass AR, Hilsenrath E, Bhartia PK, Beer R, Waters JW, Gunson MR, Froidevaux L, Gille JC, Barnett JJ, Levelt PF (2006) Overview of the EOS Aura mission'. IEEE Trans Geosci Remote Sens 44(5):1066–1074

14. Doll CN, Muller JP, Elvidge CD (2000) Nighttime imagery as a tool for global mapping of socioeconomic parameters and greenhouse gas emissions. Ambio 157−162

15. Welton EJ, Voss KJ, Quinn PK, Flatau PJ, Markowicz K, Campbell JR, Spinhirne JD, Gordon HR, Johnson JE (2002) Measurements of aerosol vertical profiles and optical properties during INDOEX 1999 using micropulse lidars. J Geophys Res Atmos 107(D19):INX2–18

16. OMI team (2012) Ozone monitoring instrument (OMI) data user's guide. NASA, Washington DC

17. Jackson JM, Liu H, Laszlo I, Kondragunta S, Remer LA, Huang J, Huang HC (2013) Suomi-NPP VIIRS aerosol algorithms and data products. J Geophys Res Atmos 118(22):12–673

18. Hsu NC, Lee J, Sayer AM, Kim W, Bettenhausen C, Tsay SC (2019) VIIRS Deep Blue aerosol products over land: extending the EOS long-term aerosol data records. J Geophys Res Atmos 124(7):4026–4053

19. Sawyer V, Levy RC, Mattoo S, Cureton G, Shi Y, Remer LA (2020) Continuing the MODIS dark target aerosol time series with VIIRS. Remote Sens 12(2):308

20. Bell ML, McDermott A, Zeger SL, Samet JM, Dominici F (2004) Ozone and short-term mortality in 95 US urban communities, 1987–2000. JAMA 292(19):2372–2378

21. Bell ML, Dominici F (2008) Effect modification by community characteristics on the short-term effects of ozone exposure and mortality in 98 US communities. Am J Epidemiol 167(8):986–997

22. Lelieveld J, Barlas C, Giannadaki D, Pozzer AJACP (2013) Model calculated global, regional and megacity premature mortality due to air pollution. Atmos Chem Phy 13(14):7023–7037
23. Amnuaylojaroen T, Macatangay RC, Khodmanee S (2019) Modeling the effect of VOCs from biomass burning emissions on ozone pollution in upper Southeast Asia. Heliyon 5(10):e02661
24. Sonkaew T, Macatangay R (2015) Determining relationships and mechanisms between tropospheric ozone column concentrations and tropical biomass burning in Thailand and its surrounding regions. Environ Res Lett 10(6):065009
25. Mekaumnuaychai T, Suranowarath K, Kanabkaew T, Lalitaporn P (2020) Observations of atmospheric carbon monoxide and formaldehyde in Thailand using satellites. EnvironmentAsia 13
26. Yimlamaid A, Suranowarath K, Kanabkaew T, Lalitaporn P (2020) Long-term assessment of daily atmospheric nitrogen dioxide in Thailand using satellite observed data. EnvironmentAsia 13
27. Buntoung S, Webb AR (2010) Comparison of erythemal UV irradiances from ozone monitoring instrument (OMI) and ground-based data at four Thai stations. J Geophys Res Atmos 115(D18)
28. Lee J, Choi WJ, Kim DR, Kim SY, Song CK, Hong JS, Hong Y, Lee S (2013) The effect of ozone and aerosols on the surface erythemal UV radiation estimated from OMI measurements. Asia Pac J Atmos Sci 49(3):271–278
29. Mehta M, Singh R, Singh A, Singh N (2016) Recent global aerosol optical depth variations and trends—a comparative study using MODIS and MISR level 3 datasets. Remote Sens Environ 181:137–150
30. Hutchison KD, Smith S, Faruqui S (2004) The use of MODIS data and aerosol products for air quality prediction. Atmos Environ 38(30):5057–5070
31. Wei J, Peng Y, Mahmood R, Sun L, Guo J (2019) Intercomparison in spatial distributions and temporal trends derived from multi-source satellite aerosol products. Atmos Chem Phys 19(10):7183–7207
32. Sukitpaneenit M, Oanh NTK (2014) Satellite monitoring for carbon monoxide and particulate matter during forest fire episodes in Northern Thailand. Environ Monit Assess 186(4):2495–2504
33. Kanabkaew T (2013) Prediction of hourly particulate matter concentrations in Chiangmai, Thailand using MODIS aerosol optical depth and ground-based meteorological data. EnvironmentAsia 6(2)
34. Sayer AM, Hsu NC, Hsiao TC, Pantina P, Kuo F, Ou-Yang CF, Holben BN, Janjai S, Chantara S., Wang SH, Loftus AM (2016) In-situ and remotely-sensed observations of biomass burning aerosols at Doi Ang Khang, Thailand during 7-SEAS/BASELInE 2015. Aerosol Air Qual Res 16(11):2786−2801
35. Nguyen TT, Pham HV, Lasko K, Bui MT, Laffly D, Jourdan A, Bui HQ (2019) Spatiotemporal analysis of ground and satellite-based aerosol for air quality assessment in the Southeast Asia region. Environ Pollut 255:113106
36. Cheewaphongphan P, Garivait S (2013) Bottom up approach to estimate air pollution of rice residue open burning in Thailand. Asia Pac J Atmos Sci 49(2):139–149
37. Vongruang P, Pimonsree S (2020) Biomass burning sources and their contributions to PM10 concentrations over countries in mainland Southeast Asia during a smog episode. Atmos Environ 228:117414
38. Lalitaporn P, Boonmee T (2019) Analysis of tropospheric nitrogen dioxide using satellite and ground based data over Northern Thailand. Eng J 23(6):19–35
39. Takemura T, Nakajima T, Dubovik O, Holben BN, Kinne S (2002) Single-scattering albedo and radiative forcing of various aerosol species with a global three-dimensional model. J Clim 15(4):333–352
40. Wang J, Virkkula A, Gao Y, Lee S, Shen Y, Chi X, Nie W, Liu Q, Xu Z, Huang X, Wang T (2017) Observations of aerosol optical properties at a coastal site in Hong Kong, South China. Atmos Chem Phys 17(4):2653–2671
41. Levoni C, Cervino M, Guzzi R, Torricella F (1997) Atmospheric aerosol optical properties: a database of radiative characteristics for different components and classes. Appl Opt 36(30):8031–8041

42. Bridhikitti A, Overcamp TJ (2011) Optical characteristics of southeast Asia's regional aerosols and their sources. J Air Waste Manag Assoc 61(7):747–754

43. Park JU, Kim SW, Sheridan PJ, Williams A, Chambers SD (2020) Long-term variability of aerosol optical properties at Mauna Loa. Aerosol Air Qual Res 20(7):1700–1711

44. Reidmiller DR, Hobbs PV, Kahn R (2006) Aerosol optical properties and particle size distributions on the east coast of the United States derived from airborne in situ and remote sensing measurements. J Atmos Sci 63(3):785–814

45. Bhaskar VV, Safai PD, Raju MP (2015) Long term characterization of aerosol optical properties: implications for radiative forcing over the desert region of Jodhpur, India. Atmos Environ 114:66–74

46. Zhang M, Ma Y, Gong W, Liu B, Shi Y, Chen Z (2018) Aerosol optical properties and radiative effects: assessment of urban aerosols in central China using 10-year observations. Atmos Environ 182:275–285

47. Kaskaoutis DG, Sinha PR, Vinoj V, Kosmopoulos PG, Tripathi SN, Misra A, Sharma M, Singh RP (2013) Aerosol properties and radiative forcing over Kanpur during severe aerosol loading conditions. Atmos Environ 79:7–19

48. Tiwari S, Pandithurai G, Attri SD, Srivastava AK, Soni VK, Bisht DS, Kumar VA, Srivastava MK (2015) Aerosol optical properties and their relationship with meteorological parameters during wintertime in Delhi, India. Atmos Res 153:465–479

49. Luoma K, Virkkula A, Aalto P, Petäjä T, Kulmala M (2019) Over a 10-year record of aerosol optical properties at SMEAR II. Atmos Chem Phys 19(17):11363–11382

50. Wang T, Du Z, Tan T, Xu N, Hu M, Hu J, Guo S (2019) Measurement of aerosol optical properties and their potential source origin in urban Beijing from 2013–2017. Atmos Environ 206:293–302

51. Chand D, Guyon P, Artaxo P, Schmid O, Frank GP, Rizzo LV, Mayol-Bracero OL, Gatti LV, Andreae MO (2006) Optical and physical properties of aerosols in the boundary layer and free troposphere over the Amazon Basin during the biomass burning season. Atmos Chem Phys 6(10):2911–2925

52. Li C, Tsay SC, Hsu NC, Kim JY, Howell SG, Huebert BJ, Ji Q, Jeong MJ, Wang SH, Hansell RA, Bell SW (2013) Characteristics and composition of atmospheric aerosols in Phimai, central Thailand during BASE-ASIA. Atmos Environ 78:60–71

53. Gautam R, Hsu NC, Eck TF, Holben BN, Janjai S, Jantarach T, Tsay SC, Lau WK (2013) Characterization of aerosols over the Indochina peninsula from satellite-surface observations during biomass burning pre-monsoon season. Atmos Environ 78:51–59

54. Sayer AM, Hsu NC, Eck TF, Smirnov A, Holben BN (2014) AERONET-based models of smoke-dominated aerosol near source regions and transported over oceans, and implications for satellite retrievals of aerosol optical depth. Atmos Chem Phys 14(20):11493–11523

55. Ebert M, Weinbruch S, Rausch A, Gorzawski G, Helas G, Hoffmann P, Wex H (2002) Complex refractive index of aerosols during LACE 98 as derived from the analysis of individual particles. J Geophys Res Atmos 107(D21):8121. https://doi.org/10.1029/2000JD000195

56. Schkolnik G, Chand D, Hoffer A, Andreae MO, Erlick C, Swietlicki E, Rudich Y (2007) Constraining the density and complex refractive index of elemental and organic carbon in biomass burning aerosol using optical and chemical measurements. Atmos Environ 41(5):1107–1118

57. Duc HN, Bang HQ, Quan NH, Quang NX (2021) Impact of biomass burnings in Southeast Asia on air quality and pollutant transport during the end of the 2019 dry season. Environ Monit Assess 193(9):1–28

58. Kamthonkiat D, Thanyapraneedkul J, Nuengjumnong N, Ninsawat S, Unapumnuk K, Vu TT (2021) Identifying priority air pollution management areas during the burning season in Nan Province, Northern Thailand. Environ Dev Sustain 23(4):5865–5884

59. Tsay SC, Hsu NC, Lau WKM, Li C, Gabriel PM, Ji Q, Holben BN, Welton EJ, Nguyen AX, Janjai S, Lin NH (2013) From BASE-ASIA toward 7-SEAS: a satellite-surface perspective of boreal spring biomass-burning aerosols and clouds in Southeast Asia. Atmos Environ 78:20–34

60. UN Economic and Social Commission for Asia and the Pacific, UN ESCAP (2021) Deciphering the black box of air pollution data in Thailand. https://www.unescap.org/blog/deciphering-black-box-air-pollution-data-thailand. Accessed on 26 January 2021
61. Huang K, Fu JS, Hsu NC, Gao Y, Dong X, Tsay SC, Lam YF (2013) Impact assessment of biomass burning on air quality in Southeast and East Asia during BASE-ASIA. Atmos Environ 78:291–302
62. Bridhikitti A (2013) Atmospheric aerosol layers over Bangkok Metropolitan Region from CALIPSO observations. Atmos Res 127:1–7
63. Kanniah KD, Lim HQ, Kaskaoutis DG, Cracknell AP (2014) Investigating aerosol properties in Peninsular Malaysia via the synergy of satellite remote sensing and ground-based measurements. Atmos Res 138:223–239
64. Liao Q, Zhu M, Wu L, Pan X, Tang X, Wang Z (2020) Deep learning for air quality forecasts: a review. Curr Pollut Rep 6(4):399–409
65. Zhang H, Wang J, García LC, Ge C, Plessel T, Szykman J, Murphy B, Spero TL (2020) Improving surface PM2.5 forecasts in the United States using an ensemble of chemical transport model outputs: 1. bias correction with surface observations in nonrural areas. J Geophys Res Atmos 125(14):e2019JD032293
66. Werner M, Kryza M, Guzikowski J (2019) Can data assimilation of surface PM2.5 and Satellite AOD improve WRF-Chem forecasting? A case study for two scenarios of particulate air pollution episodes in Poland. Remote Sens 11(20):2364
67. Hollingsworth A, Engelen RJ, Textor C, Benedetti A, Boucher O, Chevallier F, Dethof A, Elbern H, Eskes H, Flemming J, Granier C (2008) Toward a monitoring and forecasting system for atmospheric composition: the GEMS project. Bull Am Meteorol Soc 89(8):1147–1164
68. Sharma E, Deo RC, Soar J, Prasad R, Parisi AV, Raj N (2022) Novel hybrid deep learning model for satellite based PM10 forecasting in the most polluted Australian hotspots. Atmos Environ 279:119111
69. Li C, Hsu NC, Tsay SC (2011) A study on the potential applications of satellite data in air quality monitoring and forecasting. Atmos Environ 45(22):3663–3675
70. SERVIR-Mekong (2021) Mekong air quality explorer. https://aqatmekong-servir.adpc.net/en/home/. Accessed on 22 August 2021

Dr. Arika Bridhikitti is an assistant professor in the Environmental Engineering and Disaster Management Program at Mahidol University Kanchanaburi Campus, Thailand. Her research includes remote sensing applications for monitoring air pollution and land use changes. She also worked on the hydrogeological processes of small to large-scale watersheds via field monitoring and modeling. Her recent research has focused on environmental monitoring in tropical forests and agroecosystems.